

Supplementary information: Ultra stable superatomic structure of doubly magic Ga₁₃ and Ga₁₃Li electrolyte[†]

Krista G. Steenbergen^{*a} and Nicola Gaston^b

^a The MacDiarmid Institute for Advanced Materials and Nanotechnology, School of Chemical and Physical Sciences, Victoria University of Wellington, P.O. Box 600, Wellington, New Zealand; E-mail: kgsteen@gmail.com

^b The MacDiarmid Institute for Advanced Materials and Nanotechnology, Department of Physics, The University of Auckland, Private Bag 92019, Auckland, New Zealand.

S1 Theoretical and Analysis Methods

We perform density functional theory (DFT) relaxations (parameters given in overview in the manuscript) for each charge state of the 13-atom cluster in order to determine a low-energy starting structure for subsequent Born-Oppenheimer DFT molecular dynamics (MD) simulations. Using DFT-MD, we model the effect of temperature. The lowest-energy isomer of each charge state is used to seed 10 ps canonical DFT-MD simulations. These canonical MD simulations are used only to equilibrate the cluster at a range of finite temperatures, including: 37 temperatures spanning 200–1540 K for Ga_{13}^- ; 33 temperatures from 200–1460 K for Ga_{13} ; and 33 temperatures from 200–1620 K for Ga_{13}^+ . The thermalised clusters from each canonical trajectory are then used as the initial structures in subsequent microcanonical simulations. The average temperature of the microcanonical trajectories match those of the canonical simulations to within 20 K.

For the microcanonical simulations, we employ a parallel tempering algorithm^{1,2} to enhance the ergodicity of the simulations, and calculate specific heat curves by the multiple histogram (MH) method.^{2–4} Using a specific heat convergence criteria described in our previous work,² the microcanonical simulations include 200 ps per temperature for Ga_{13}^- and Ga_{13} , and 300 ps per temperature for Ga_{13}^+ . Additional details of the parallel tempering and MH mathematical development are given in our previous works.^{2,5–9}

This method has been benchmarked for gallium clusters by direct comparison to experimental results,^{10–12} for both the clusters^{2,5–9} and bulk gallium.⁷ The remarkable similarity between the detailed features of the simulated and experimental specific heat curves demonstrates the accuracy of our methods.⁵ Compared to experiment, we observe a consistent shift -90 K shift in the simulated melting temperatures for both the clusters⁵ and bulk,⁷ which we attribute to an energetic shift of the PW91 functional for gallium nanoclusters and bulk.

In order to analyse cluster geometric structure at finite temperature, we utilise three mathematical tools. The first tool is the principal component analysis (PCA) which allows us to determine the three principal axes of a cluster, \mathbf{P}_1 , \mathbf{P}_2 and \mathbf{P}_3 .⁸ These axes define the longest cluster dimension, second longest orthogonal cluster dimension and the shortest orthogonal cluster dimension, respectively. We use these axes to measure the lengths of the longest, middle and shortest (principal) cluster dimensions, designated l_1 , l_2 and l_3 , respectively. The PCA enables us to analyze the overall cluster shape at every finite temperature MD time step, and easily identify isomerisations that result in overall shape changes^{6–8} over the course of MD trajectories that generate hundreds of thousands of structures. We have used the PCA to track structural changes and determine the dominant polymorph at any given finite temperature.^{6,8}

The second tool is a short-time average of the pair distribution function (taPDF) combined with a Pearson Correlation Coefficient (PCC) analysis. Here, we calculate the traditional pair distribution function histogram of bond lengths for the cluster structure at every MD time step, then average the histograms over 5 MD time steps. The taPDF gives us a bonding signature that captures the finite temperature fluctuations of the cluster structures. We can then statistically compare these signatures between different cluster charge states using the correlation analysis outlined by Pearson.^{8,13} A PCC of +1 would indicate perfect correlation of bonding signatures, while anything >0.9 indicates a very strong positive correlation. Our previous work gives more mathematical detail of the PCA, taPDF and PCC.⁸

The third analysis tool is a planar-projected average cluster structure. Given an orthorhombic simulation box defined by the lattice vectors $(\vec{X}, \vec{Y}, \vec{Z})$, we choose two dimensions to create a rectangular (or square) area – for example, a rectangular defined by (\vec{X}, \vec{Y}) . We then draw 19 grid lines (20 divisions) for each dimension, creating a 20×20 grid. For each MD time step, a tally is made in each grid box where the (x, y) coordinate of an atom falls within the grid boundaries. For this tallying, the z coordinate is ignored, essentially making the measure a histogram of the cluster structure projected onto the x - y plane. For consistency between histograms, we divide the final bin counts by the total number of structures tallied (MD time steps), giving a measure of the percentage of time an atom is found within any bin. The projection can be done onto any plane (x - y , x - z or y - z). For the liquid structures, where the finite temperature fluctuations in geometric structure are typically extreme, we combine this measure with the PCA analysis, such that the lattice vectors are no longer defined by $(\vec{X}, \vec{Y}, \vec{Z})$, but by the principal axes of the cluster structure $(\mathbf{P}_1, \mathbf{P}_2, \mathbf{P}_3)$. For the solid clusters, we have applied a simple coordinate rotation at every MD time step such that: the vector between the central atom and one of the decahedral vertex atoms aligns parallel to the y -axis; the vector between the central atom and another decahedral vertex atom makes as small an angle as possible with the x -axis.

S2 Correlation results for neutral and anion

We compare the Pearson Correlation Coefficients of the taPDF's (described above) between the neutral and anionic clusters. For temperatures below 500 K, the anion and neutral taPDFs exhibit a very strong positive correlation, with an average PCC^{8,13} > 0.92.

S3 Supplemental figures

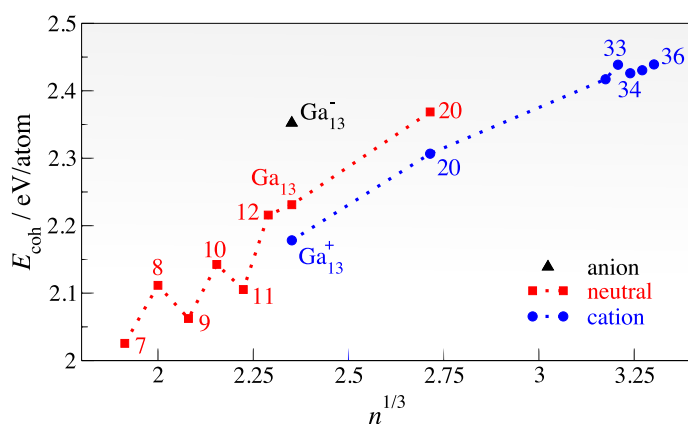


Fig. S1 The cohesive energy of the lowest-energy 13-atom clusters as a function of the cube-root of the number of atoms (n). As a reference, we give E_{coh} of other simulated gallium cluster sizes and charge states.

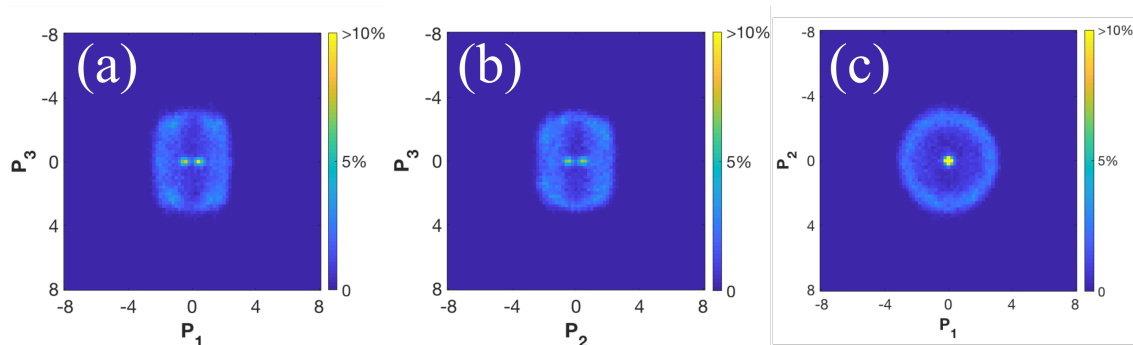


Fig. S2 The average cluster structure for Ga_{13}^+ at ~ 300 K below T_m (~ 700 K). Here, we use the PCA to rotate the cluster into the \mathbf{P}_1 - \mathbf{P}_2 - \mathbf{P}_3 coordinate reference at every MD time step. In order to give the full pictures of the average cluster structure, we give all three planar projections: (a) the longest and shortest axes (\mathbf{P}_1 - \mathbf{P}_3 plane), (b) the second-longest and shortest (\mathbf{P}_2 - \mathbf{P}_3 plane), and (c) the longest and second-longest (\mathbf{P}_1 - \mathbf{P}_2 plane). The overall flattened nature of the cation is clear from plots (a) and (b); however, (c) clearly illustrates that the spherical nature with the same surface degeneracy observed for the neutral and anion is also maintained.

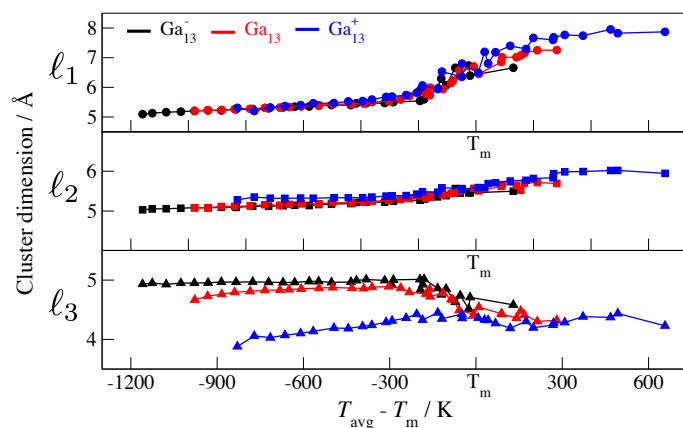


Fig. S3 Comparing the average cluster dimension at each simulated average temperature. The temperature scale for each cluster has been shifted such that the solid-liquid transition for each charge state is the same (referenced as T_m). Note that the average liquid dimensions of all three charge states are nearly identical, indicating that the charge affects the liquid state to a negligible degree. Comparing the neutral and anion solid clusters, the average dimensions differ only by ~ 0.1 Å in the l_3 dimension, illustrating that the overall geometric shape of the clusters is nearly identical throughout the solid phase. The cation's l_1 and l_2 match those of the anion and neutral clusters; however, the cation's l_3 dimension is shortened by ~ 1 Å in the solid phase, illustrating the flattened nature of the cation.

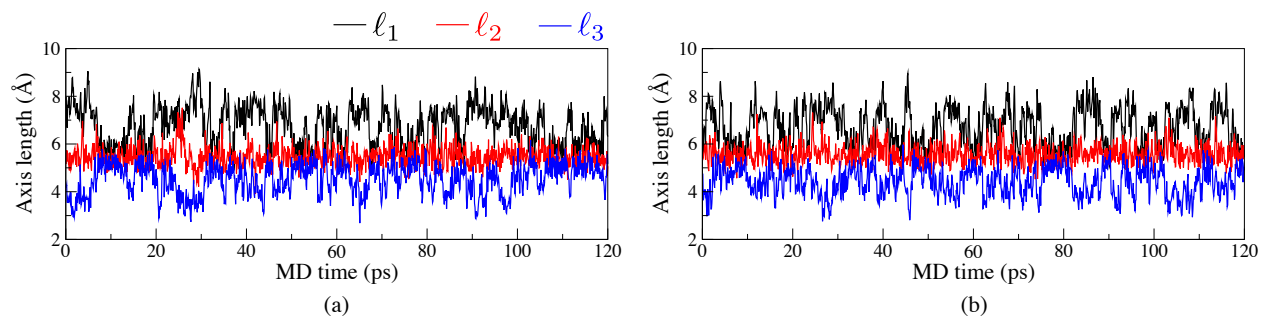


Fig. S4 The PCA results for the cluster structure at every MD time step in a trajectory at $T_m + 200\text{ K}$ for the (left) Ga_{13}^- anion and (right) Ga_{13} neutral, illustrating metastable, highly-elongated states that last for up to 10 ps. At higher liquid temperatures, the 2D metastable states dominate the MD trajectories. Although not displayed, the cation exhibits the same 2D liquid structure.

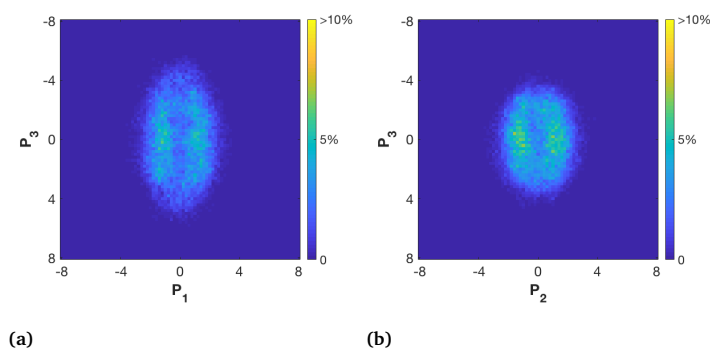


Fig. S5 The average liquid structure Ga_{13}^+ at $T_m + 500\text{ K}$ from two perspectives, illustrating the 3 average dimensions of the cluster. From both perspectives, we note the higher probability of finding atoms in one of two planes of the liquid structures. Although given only for the cation, the neutral and anion liquids have the same average liquid structures.

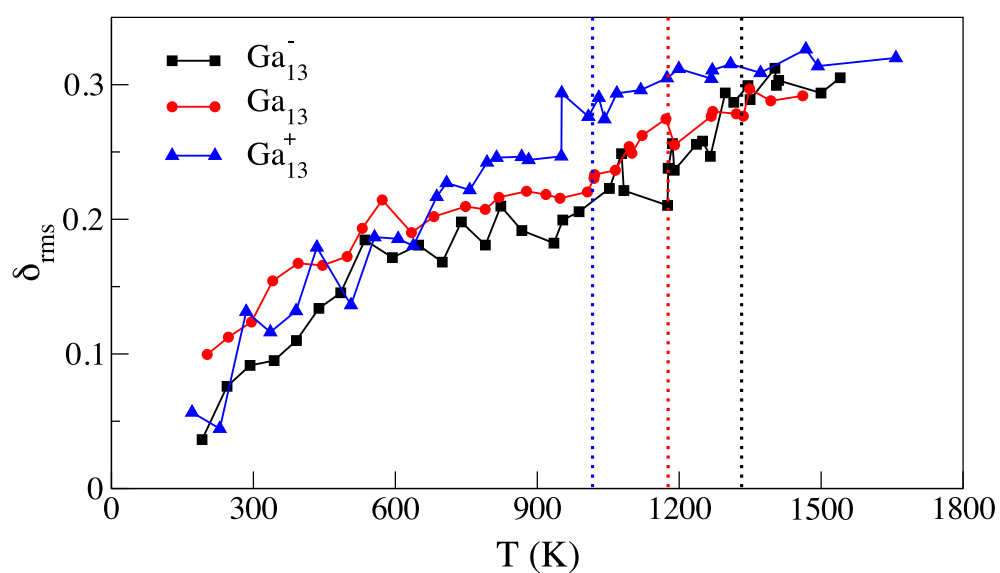


Fig. S6 The root-mean square bond length variance (δ_{rms}) as a function of average temperature. We note the region from ~ 500 K up to ~ 200 K prior to melting, where the slope of each curve flattens – this region corresponds to the temperatures of structural reconfiguring between icosahedral and decahedral, as described in the main text.

Notes and references

- 1 F. Calvo, J. P. Neirotti and D. L. Freeman, *J. Chem. Phys.*, 2000, **112**, 10350–10357.
- 2 K. G. Steenbergen, D. Schebarchov and N. Gaston, *J. Chem. Phys.*, 2012, **137**, 144307–12.
- 3 N. Metropolis and A. W. Rosenbluth, *J. Chem. Phys.*, 1953, **21**, 1087–1092.
- 4 F. Calvo and P. Labastie, *Chem. Phys. Lett.*, 1995, **247**, 395–400.
- 5 K. G. Steenbergen and N. Gaston, *Phys. Rev. B*, 2013, **88**, 161402–5.
- 6 K. G. Steenbergen and N. Gaston, *Chem. Eur. J.*, 2014, **21**, 2862–2869.
- 7 K. G. Steenbergen and N. Gaston, *Nano Lett.*, 2016, **16**, 21–26.
- 8 K. G. Steenbergen and N. Gaston, *J. Chem. Phys.*, 2014, **140**, 064102–7.
- 9 K. G. Steenbergen and N. Gaston, *Phys. Chem. Chem. Phys.*, 2013, **15**, 15325–9.
- 10 G. A. Breaux, D. A. Hillman, C. M. Neal, R. C. Benirschke and M. F. Jarrold, *J. Am. Chem. Soc.*, 2004, **126**, 8628–8629.
- 11 G. A. Breaux, B. Cao and M. F. Jarrold, *J. Phys. Chem. B*, 2005, **109**, 16575–16578.
- 12 K. L. Pyfer, J. O. Kafader, A. Yalamanchali and M. F. Jarrold, *J. Phys. Chem. A*, 2014, **118**, 4900–4906.
- 13 K. Pearson, *Philos. Mag.*, 1901, **2**, 559–572.